Applied Energy 253 (2019) 113506

Contents lists available at ScienceDirect

Applied Energy

journal homepage: www.elsevier.com/locate/apenergy

Thermally responsive coating on building heating and cooling energy efficiency and indoor comfort improvement

Cheng Wang[a,*], Ye Zhu[b], Xiaofeng Guo[c,d,*]

[a] Jiangsu Provincial Key Laboratory of Oil & Gas Storage and Transportation Technology, Changzhou University, Changzhou 213164, Jiangsu, PR China
[b] Jiangsu Provincial Key Laboratory of Fine Petrochemical Engineering, Changzhou University, Changzhou 213164, Jiangsu, PR China
[c] ESIEE Paris, University of Paris Est, 2 boulevard Blaise Pascal – Cité Descartes, F-93162 Noisy Le Grand, France
[d] University of Paris Diderot, Sorbonne Paris Cité, LIED, UMR 8236, CNRS, F-75013 Paris, France

HIGHLIGHTS

- Optic-Variable Wall (OVW) allows HVAC energy-saving and comfort improvement in buildings.
- Up to 15% cooling in Shanghai and 7% heating in Paris can be saved thanks to OVW.
- Both overheat and overcold discomfort are reduced in the two climate conditions.
- Meteorological conditions in Shanghai are more suitable for OVW application.

ARTICLE INFO

Keywords:
Optics Variable Wall
Thermally responsive coating
Dynamic simulation
Building energy saving
Thermal comfort

ABSTRACT

Optic-Variable Wall (OVW) using thermally responsive coating on the façades of high-rise residential buildings is assessed by dynamic simulation. Evaluation criteria are energy consumptions (heat flux) during heating and cooling seasons as well as human thermal comfort. For the latter, Discomfort Hours and Discomfort Degree Hours during intermediate seasons are assessed according to the reference comfort zone given by ASHARE adaptive model. Two different cities, Shanghai and Paris, are studied to comparatively assess the effect of using such a coating under the two distinct climates. Results confirm the significant energy saving potential in the order of 8% for actual-stage coating and as high as 15% for the ideal one. Thermal Discomfort Degree Hours as well as Discomfort Hours are also reduced thanks to the tuning effect of the coating. The potential use of the temperature sensitive coating at the south wall (or facing equator) has better effect than walls of other orientations. Compared with the cold climate in Paris, Shanghai has comparable heating and cooling demand and is more adapted to the future deployment of OVW: the same OVW is doubly tuned (17% v.s. 8%) in Shanghai than in Paris, contributing to HVAC saving and improved comfort.

1. Introduction

Residential building heating and cooling consumption mainly depends on building envelop, outdoor climatic conditions, as well as internal occupancy loads. Among the outdoor climatic conditions, solar radiation, air temperature, as well as wind speed are key influencing parameters [1,2]. In addition, the Urban Heat Island (UHI) effect, contributing to a local micro-climatic singularity, affects energy consumption for buildings located in high-density urban areas [3,4]. In general, methods to reduce heating and cooling loads can be divided into *passive* and *active* measures. *Passive* techniques intend to reduce the heat gain/loss when the outdoor air temperature (OAT) is far away from the human thermal comfort range specified by building codes. Better building insulation [5–7], impermeability and the use of double-layer glass [8,9] are among these methods. In addition, effective building energy management (BEM) system together with occupants' collaboration are also crucial [10,11]. *Active* techniques act at the energy system level, trying to make use of high energy efficiency technologies, from heat pump [12,13], heat recovery [14,15] or cold recovery [16], to integration of renewable technologies [17,18], etc. At the district scale, the interaction of energy-water [19] or energy-food [20] has also attracted attention as they offer new opportunities

* Corresponding authors at: Changzhou University, 1st Gehu Road, 213164 Changzhou, PR China. (C. Wang). ESIEE Paris, Department SEN, 2 bd Blaise Pascal BP99, 93162 Noisy Le Grand Cedex, France (X. Guo).
E-mail addresses: wangcheng3756@163.com (C. Wang), xiaofeng.guo@esiee.fr (X. Guo).

https://doi.org/10.1016/j.apenergy.2019.113506
Received 14 February 2019; Received in revised form 7 June 2019; Accepted 9 July 2019

towards rational urban planning [21].

Making better use of solar radiation in the building ranks among the most promising methods in recent years. More specifically, introducing more solar gain in cold seasons, or in contrary, reducing solar penetration during hot seasons, can considerably reduce heating and cooling demands. Similarly, the improvement of thermal comfort in intermediate seasons, during which no active heating or cooling is provided, is expected by better adjusting the solar heat gain. Besides common practices like the use of solar shading panel or curtain [22], recent advancements on optical properties of façades [23] as well as window glazing [24] gain increasing attention.

Zhang et al. have studied the influence of solar reflective coating on building energy needs based on the hot/humid climatic condition of Chengdu, China [25]. Based on their experimental results, for a building with *retro*-reflective coating materials (albedo = 0.59), its average indoor air temperature (IAT) is about 2.4 °C lower than the reference building without such a coating. This is mainly due to the decrement of solar radiation absorption on external walls. Similarly, Pisello et al. [26] and Morini et al. [27] investigated the passive cooling effect of cool materials (membranes or paintings) on roofs and façades at the building and urban scales, respectively. In particular, the latter [27] has confirmed the reduced UHI effect through the use of *retro*-reflective (RR) materials. Goldstein et al. [28] reported the adoption of radiative sky cooling to reject heat from a delicately-designed coating-structure to aerospace and offer cool water in day-time with clear weather. However, all the above coatings are only reflective and not temperature-dependent, which means that it is only adapted to cooling in summer instead of to all-year-through climatic conditions. Particularly during winter period, the reflective materials reduces the solar input into building and thus results in both higher heating consumption and more water condensation risk [29]. Therefore, to some extent, the non-switchable *retro*-reflective technology is limited in the scope of hot-dry climate for cooling effects. For that reason, a material that can automatically adapt to outdoor meteorological conditions of winter, summer and transitional seasons is of great application potential.

Recently, some innovations in optics applied to windows glazing offering control of solar heat gain and daylight penetration have aroused much attention. According to their mechanisms, the techniques can be classified into electrically-actuated and non-electrically-actuated materials [23]. The former includes electrochromic, liquid crystal and suspended particle device glazing systems that require electric activation; while the second category includes thermochromic, thermotropic, and gasochromic glazing systems that are temperature sensitive. For instance, “clever” glaze can automatically switch from transparent to opaque according to its temperature. Taha et al. [30] reported the development of Vanadium Dioxide (VO2) based thin film capable to dramatically change its transmissivity at around 60–70 °C. Similar materials open the possibility to smart buildings for efficient energy management and indoor comfort improvement [31].

Compared with transparent windows, opaque façades often occupy most of the building envelop and could be responsible of a large share of the total heat gain or loss, especially in old buildings. Besides, under strong solar radiation, it is more probable for a high-absorptivity opaque wall to rise up to 60–70 °C, rather than a transparent window with high transmissivity. Therefore, the current study focuses on assessing the effects of a temperature responsive smart coating on opaque façades for the reduction of heating and cooling energy consumption as well as the improvement of indoor comfort. Once heated by solar incident radiation, the reflectivity (noted as albedo hereafter) of the coating turns from a low value to a high one. This concept will be presented as Optic-Variable Wall (OVW), but it can also be named as “Temperature sensitive coating”, “Thermally responsive wall”, “Variable reflectivity coating” or “Tunable reflectivity wall”.

2. Coating properties and previous work

The development and characterization of a temperature responsive coating have been previously reported by Wang et al. [32]. The characteristic of the coating on the absorption and the reflection of solar radiation, mainly within the wavelength region of visible light, is sensible to its temperature. At high temperature, the coating shows strong reflection to the radiation exposing on the OVW; while the reflection becomes weak at low temperature.

Eq. (1) describes the albedo variation in the case of a thermally responsive coating. The albedo turns from a low value (ρ_1) to a higher one (ρ_2), when the temperature of the surface (T_{wo}) increases:

$$\rho = \begin{cases} \rho_1 \\ \rho_1 + \left(\frac{T_{wo} - T_{s1}}{T_{s2} - T_{s1}}\right)\cdot(\rho_2 - \rho_1) \\ \rho_2 \end{cases} \text{for} \begin{cases} T_{wo} \leqslant T_{s1} \\ T_{s1} \leqslant T_{wo} \leqslant T_{s2} \\ T_{wo} \geqslant T_{s2} \end{cases} \quad (1)$$

where T_{s1} and T_{s2} are respectively lower and upper tuning temperature limits. For our current lab-developed coating, the tuning temperature ranges from T_{s1} = 23.5 °C to T_{s2} = 26.5 °C. The albedo values are measured with UV–VIS-NIR (Shimadzu 3600) under controlled temperature conditions. At the actual stage, they are respectively ρ_2 = 0.45 (high temperature) and ρ_1 = 0.1 (low temperature).

Several applications have already been investigated in our earlier works. Applying the OVW on a container has been experimentally confirmed effective in the internal air temperature control [32]. The temperature rise in the container, in case of strong solar explosion, can be as low as 5 °C using the OVW while that of an absorptive wall will jump by as high as 15 °C. In a more recent work reported by the same authors [33], the OVW is shown to be able to offer a cumulative heat flux reduction as high as 158.4 kWh/m^2 through a façade. This implies potentially significant energy saving and temperature auto-regulation thanks to this coating.

In the two previous works, only the effects on a simplified box or façade are investigated. Yet, a real building should be dynamically modelled by considering several differently oriented façades as well as internal heat gains. In addition, indoor thermal comfort, which is another important criterion for building application, should be taken into account.

The current manuscript reports a rigorous annual dynamic simulation that allows detailed evaluation of such a coating on a simplified residential building. Two Northern hemisphere cities, Paris and Shanghai, are chosen to comparatively assess the adaptivity of the coating under difference climates. The two cities are typically representative to cover a large percentage of urban areas in the world. Furthermore, to directly identify the most appropriate façade orientation, the OVW is applied both to the East and to the South walls for comparison. In the current model, we adopt two OVW properties and a fixed tuning temperature range. The first one is the properties of our lab prepared samples in the actual stage (noted as *actual* hereafter), with respectively ρ_1 = 0.1 and ρ_2 = 0.45. The second sample properties are ideal values that are theoretically achievable. Noted as *ideal*, its albedo range is from ρ_1 = 0.1 to ρ_2 = 0.8. For both samples, the tuning temperature range is the same, i.e., from T_{s1} = 23.5 °C to T_{s2} = 26.5 °C. Out of this range, the coating is either highly absorptive at lower temperatures or highly reflective once heated to higher level (by solar radiation and convective heat exchange with outdoor ambient).

3. Modelling method and procedure

3.1. Heat flux equation

As in an urban context, high-rise buildings are chosen as the object in our analysis. Roofs and grounds are not considered so that the focus is only given to walls. The heat flux through a standard wall subjected to beam solar irradiance can be represented by the model schematized

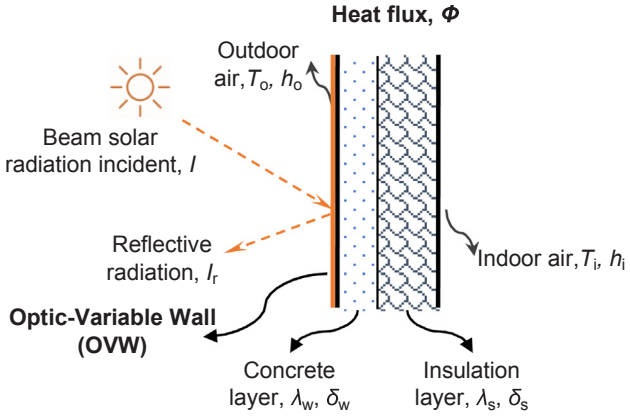

Fig. 1. Heat flux through an optic-variable wall with two layers and thermally responsive coating on the exterior side.

in Fig. 1, considering interior and exterior convection as well as the heat conduction through two layers (concrete and insulation).

Under a given solar irradiance I on a vertical surface, the heat flux from exterior to interior of a unit area, double-layer wall can be expressed as:

$$\Phi = \frac{(1-\rho)\cdot I - h_o\cdot(T_i - T_o)}{1 + \left(\frac{1}{h_i} + \frac{\delta_w}{\lambda_w} + \frac{\delta_s}{\lambda_s}\right)\cdot h_o} \tag{2}$$

where, ρ represents the reflectivity of the façade, h_i and h_o respectively convective heat transfer coefficient for the inner wall and outer façade, W/(m^2·°C), T_i and T_o are IAT (Inside Air Temperature) and OAT (Outside Air Temperature), °C; δ_w and δ_s are respectively wall and insulation layer thickness, m; and λ_w, λ_s the heat conductivity of respectively wall and insulation layer, W/(m·°C).

In the above expression, no IR radiative heat transfer is considered but only the global solar beam radiation comprising of direct and ground-reflected terms. The function remains valid when the beam solar radiation is null ($I = 0$) and negative Φ value means heat loss from indoor to outdoor of the wall.

Since the outer wall temperature T_{wo} is also closely coupled with solar irradiance, when IAT is prescribed in the stationary heat transfer, we developed an explicit relationship between the solar irradiance and the albedo as shown in Eq. (3) through Eq. (5).

For absorptive albedo at low temperature, we use Eq. (3):

$$\rho = \rho_1 \text{if } I \leqslant \frac{1}{(1-\rho_1)}\cdot\left(\frac{T_{s1} - T_i}{\frac{1}{h_i} + \frac{\delta_w}{\lambda_w} + \frac{\delta_s}{\lambda_s}} + h_o\cdot(T_{s1} - T_o)\right) \tag{3}$$

For intermediate temperature range, the albedo value is determined, between ρ_1 and ρ_2, by Eq. (4):

$$\rho = \rho_1 + (\rho_2 - \rho_1)\cdot\frac{(T_i - T_{s1}) + \left(\frac{1}{h_i} + \frac{\delta_w}{\lambda_w} + \frac{\delta_s}{\lambda_s}\right)\cdot(h_o\cdot(T_o - T_{s1}) + (1-\rho_1)\cdot I)}{(T_{s2} - T_{s1}) + \left(\frac{1}{h_i} + \frac{\delta_w}{\lambda_w} + \frac{\delta_s}{\lambda_s}\right)\cdot(h_o\cdot(T_{s2} - T_{s1}) + (\rho_2 - \rho_1)\cdot I)} \text{if}$$
$$\frac{1}{(1-\rho_1)}\cdot\left(\frac{T_{s1} - T_i}{\frac{1}{h_i} + \frac{\delta_w}{\lambda_w} + \frac{\delta_s}{\lambda_s}} + h_o\cdot(T_{s1} - T_o)\right) \leqslant I \leqslant \frac{1}{(1-\rho_2)}\cdot$$
$$\left(\frac{T_{s2} - T_i}{\frac{1}{h_i} + \frac{\delta_w}{\lambda_w} + \frac{\delta_s}{\lambda_s}} + h_o\cdot(T_{s2} - T_o)\right) \tag{4}$$

Finally, in the case of higher temperature, the OVW becomes reflective through Eq. (5):

$$\rho = \rho_2 \text{if } I \geqslant \frac{1}{(1-\rho_2)}\cdot\left(\frac{T_{s2} - T_i}{\frac{1}{h_i} + \frac{\delta_w}{\lambda_w} + \frac{\delta_s}{\lambda_s}} + h_o\cdot(T_{s2} - T_o)\right) \tag{5}$$

3.2. Evaluation criteria

As performance indicators, we use energy consumption quantities during heating and cooling seasons and discomfort indicators during intermediate seasons. In the latter case, the indoor environment is not actively controlled by HVAC but only subject to external & internal thermal loads.

3.2.1. HVAC energy consumption

During heating and cooling seasons, HVAC energy consumptions are used for comparison. For heating, the heating element (gas furnace or electric radiator) is supposed to hold a fixed heating power of 2 kW. Regarding its control, the heating target IAT is set to 20 °C, with a ON/OFF differential controller dead-band of ± 1 °C. Concerning cooling, the cooling power of the air-conditioner is also set to 2 kW, with a target indoor air temperature of 26 °C and dead-band of ± 1 °C. The heating and cooling powers are then integrated in their corresponding operation seasons to finally yield the respective annual energy consumptions.

3.2.2. Adaptive comfort zone

A diversity of methods can describe the thermal comfort issue in buildings. First, the Discomfort Hours (DH) number can quantify the sum of discomfort time duration [34–36]. It can be used either in an absolute basis or in the form of relative percentage values. Meanwhile, this parameter does not consider the degree of discomfort (heat or cold stress). Second, Zhang et al. [37] introduced the use of overheat and overcool Discomfort Degree Hours (DDH) during summer and winter in a free ventilation building. The DDH takes into account not only the discomfort duration but the temperature difference till the ideal comfortable temperature limit. The method is recently used by Lin et al. [38] as an optimization objective in a building thermal load and discomfort prediction modelling. Another method is the PMV and PPD association capable to evaluate the thermal comfort for different building typologies and considering the occupants metabolisms. The model has been pioneered by Fanger [39] and is widely adopted in European and ISO standards through EN 15251 [40,41] and ISO 7730 [42,43]. Nevertheless, these parameters are usually used in HVAC-controlled buildings and mainly during heating/cooling seasons. Moreover, the PMV is often accused to not be able to sufficiently represent individual votes, especially for buildings with natural ventilation [41,44].

In this study, we adopt another widely used model, i.e., the adaptive comfort model. The model has been developed and revised by ASHRAE [45,46]. It distinguishes natural ventilated seasons with HVAC controlled ones and gives comfort satisfactory zones (90% and 80%) according to OAT (Outdoor Air Temperature).

In a natural convection building, the adaptive model gives the following comfort indoor temperature values shown in Eq. (6):

$$T_i = 18.9 + 0.255T_o \tag{6}$$

Then, based on statistical studies, a 90% satisfaction zone is defined in Eq. (7) with a temperature fluctuation of ± 2.79 °C:

$$T_{i,90\%} = 18.9 + 0.255T_o \pm 2.79 \tag{7}$$

Similarly, the zone for a statistical 80% satisfaction is given by Eq. (8):

$$T_{i,80\%} = 18.9 + 0.255T_o \pm 3.27 \tag{8}$$

For HVAC controlled building (summer and winter), the comfort is also defined. Since in our case, the HVAC during heating and cooling seasons are supposed to be ideally controlled and 24 h running, thermal comfort is considered as guaranteed. The room temperature is maintained respectively as 20 °C for winter and 26 °C for summer. For these periods, only energy consumption due to HVAC is considered and compared.

3.2.3. Discomfort Degree-Hour

We also use DDH and DH to represent the thermal (dis)comfort indices exclusively during the intermediate, no HVAC seasons. The DDH characterize both the time duration and the discomfort degree, i.e., the difference between IAT with the ideal one defined by the adapted model. Whereas the DH only represents the time accumulation of the discomfort out of the 80% satisfactory zone given by the adaptive model.

More specifically, we use the following parameters to evaluate the discomfort, based on the adaptive comfort zone concept: i) DDH, Discomfort Degree Hours, including overheat Discomfort Degree Hours DDHh and overcool ones by DDHc; ii) Discomfort Hours, DH, including DHh (overheat Discomfort Hours over 80% satisfactory zone, 3.27 °C above the comfortable value given by the adaptive model) and DHc: overcool Discomfort Hours lower than 80% satisfactory range; and iii) DHhr and DHcr: representing respectively the relative overheat and overcool discomfort hours (or annual intermediate seasonal discomfort ratio) out of the total intermediate season hours (2920 h in a year).

The definitions of the above parameters are shown in equations below:

$$DHh = \sum_{1}^{t} \Delta t \quad if \quad T_i > 18.9 + 0.255T_o + 3.27 \tag{9}$$

$$DHc = \sum_{1}^{t} \Delta t \quad if \quad T_i < 18.9 + 0.255T_o - 3.27 \tag{10}$$

$$DDHh = \sum_{1}^{t} \Delta t(T_{int} - (18.9 + 0.255T_o)) \quad if \quad T_i > 18.9 + 0.255T_o \tag{11}$$

$$DDHc = \sum_{1}^{t} \Delta t(-T_{int} + (18.9 + 0.255T_o)) \quad if \quad T_i < 18.9 + 0.255T_o \tag{12}$$

where $\Delta t = 1$ h is the time step used in the simulation, and $t = 2920$ h totalizes the four-month intermediate season separated into two periods (Spring and Autumn).

3.3. Model implementation

A 75 m^2 apartment whose architectural plan is shown in Fig. 2 is modeled in TRNSYS [47]. The building has external walls facing South, East and North. In the West, the internal walls are considered to have no heat flux with the neighboring spaces. The internal height of the building has a homogeneous value of 3.2 m. The external oriented walls are composed of two layers: concrete and insulation. The coating of OVW is only applied to the East and to the South walls that receive direct solar radiation. For the rest, heat gain or heat loss are determined without the term I (Eq. (2)).

The same building architecture is considered in Shanghai and Paris respectively, which are two cities with distinctive climatic conditions in China and in France. Meteorological data of both cities are provided by TRNSYS Meteonorm [48], via the Type TM-Y.

Several hypotheses are used to simplify the modelling procedure. First, the building is considered as a mono-zone lumped model, without distinctions among living room, bedrooms and kitchens. Secondly, we consider no mechanically air ventilation or air renewal, but only the thermal mass of the internal air. Besides, a fixed internal heat load of 200 W is considered all through the year. These assumptions allow us to concentrate our investigation on key dynamic parameters, i.e., solar radiation, heat transfer flux and thermal inertia.

The U-value and heat capacitance of the building are determined as follows. U value: $h_i = 10$ W/(m^2·°C), $h_o = 30$ W/(m^2·°C), $\lambda_{concrete} = 1$ W/(m·°C), $\lambda_{insulation} = 0.046$ W/(m·°C), thickness $\delta_{concrete} = 0.25$ m and $\delta_{insulation} = 0.1$ m. Capacitance values are obtained using the following parameters: the concrete [49] has a specific heat capacity of $c_{p,\ concrete} = 1000$ J/(kg·°C), and a density of $m_{v,\ concrete} = 1500$ kg/m^3, thus $(m_v c_p)_{concrete} = 1500$ kJ/(m^3·°C). For the insulation layer, the total thermal mass is $(m_v c_p)_{insulation} = 48$ kJ/(m^3·°C).

On the basis of modelling a year from January to December, predefined HVAC (heating and cooling) and transitional seasons are used for both two cases (respectively in Shanghai and Paris). The heating season covers the period from November 15th to March 15th of the next year, and the cooling season starts from May 15th and ends on September 15th. Two periods before (Spring) and after (Autumn) the cooling period are considered as intermediate seasons (no HVAC). Together they account for 4 months in a year. Additionally, each of the two heating/cooling seasons accounts for 4 months.

The control strategy of the heating and cooling emitters is based on the differential control protocol and set points as previously described in the Section 3.2.1.

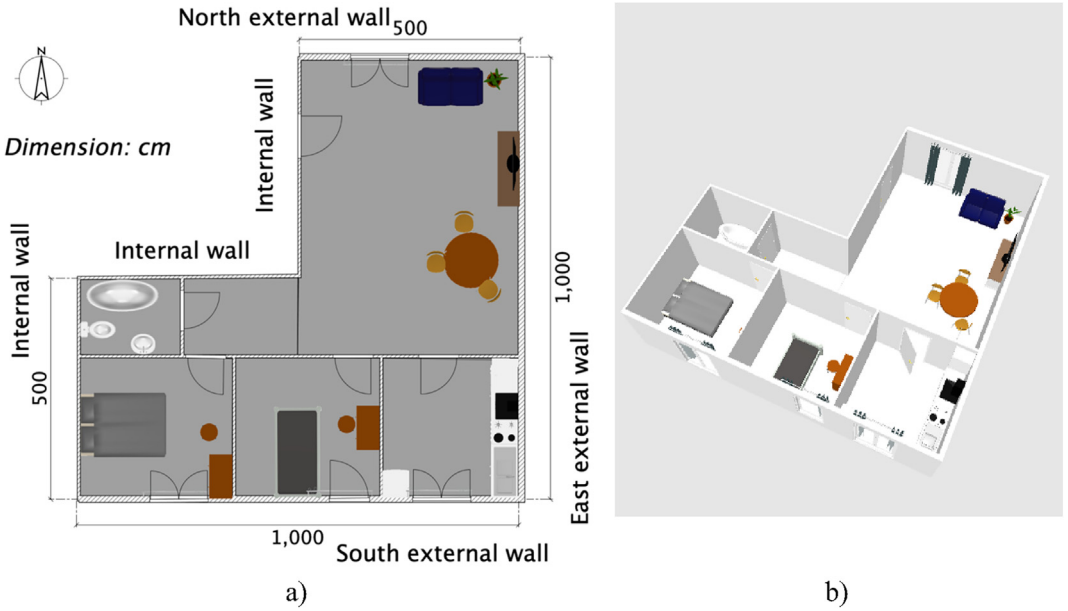

Fig. 2. The configuration of a 75 m^2 residential apartment that is taken as example, (a) building 2D plan and (b) 3D view.

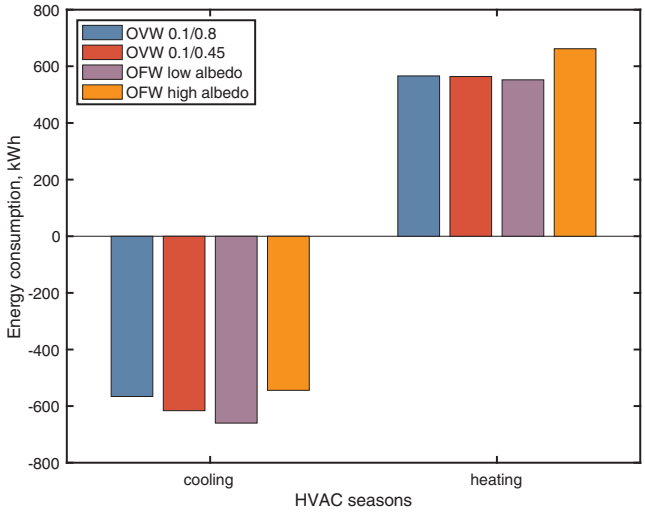

Fig. 3. Comparison of annual heating and cooling primary energy consumption (in kWh).

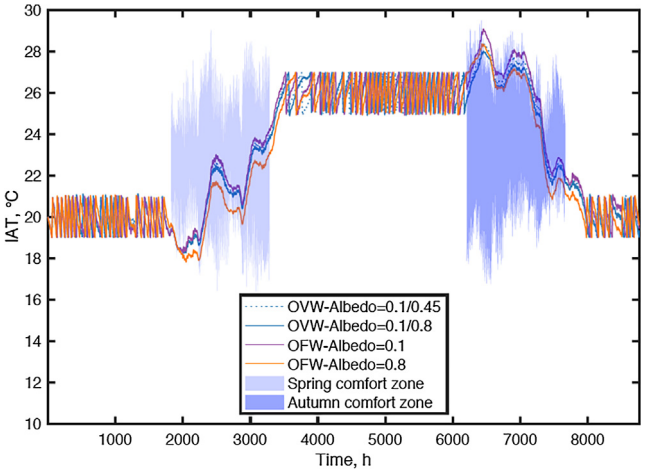

Fig. 4. Indoor air temperature all through the year, case of Shanghai *actual* OVW is shown as OVW-Albedo = 0.1/0.45, and *ideal* OVW is shown as OVW-Albedo = 0.1/0.8; OFW-Albedo = 0.1 and OFW-Albedo = 0.8 are absorptive and reflective fixed albedo surface, respectively.

4. Results and discussions

4.1. Case of Shanghai

Under the climatic condition of Shanghai (see Fig. A1 and Fig. A2 in Supplementary Data, both OAT and solar beam radiation are provided, retrieved from TRNSYS Meteonorm [47,48]), OVW can help achieve annual HVAC energy saving than both the two other OFWs (see Fig. 3). In Winter, the heating load for OVW is slightly higher than the low reflectivity OFW but much lower than the OFW with fixed higher albedo. This is due to higher solar radiation absorption during Winter thanks to the temperature dependent characteristic of OVW that is *tuned* to lower albedo values. Similarly, Summer cooling load in the case of OVW becomes lower than lower albedo OFW and approaches that of reflective OFW. This implies that OVW blocks the solar radiation absorption by turning its reflectivity during Summer.

More specifically, the actual OVW (albedo = 0.1/0.45) helps economize 8.2% of cooling demand than the absorptive wall (616 kWh v.s. 660 kWh). In the long term, the ideal OVW (albedo = 0.1/0.8) will be capable to increase the energy saving up to 14.2%, reducing the annual cooling demand to only 566 kWh. This performance is much higher than other similarly applicable energy-saving measures such as thermal paint coating. Recent study by Simpson et al. [50] estimates only energy savings of between 0.4% and 2.9% depending on coating thickness and type.

In terms of heating demand, using the actual OVW (with 0.1/0.45) and the ideal (albedo = 0.1/0.8), gives almost the same result (564 kWh for the actual one and 566 kWh for the ideal). The reason for this is that, during Winter period, the albedo remains nearby its low value, i.e., 0.1. Comparatively, fixing the albedo to 0.1, in the case of absorptive OFW, can reduce the heating demand to 552 kWh while the reflective one will result in an annual heating demand as high as 662 kWh. Therefore, using OVW reduces 14.8% of heating demand than the most unfavorable case. In conclusion, the solar radiation induced heat flux, acting as a supplementary heat contribution, has significant influence on the winter heating demand; and thanks to the use of OVW, this influence becomes *tunable*.

The annual IAT of the four cases of different wall properties are shown in Fig. 4. It worth reminding that the whole year, beginning from January and ending in December, is separated into five sequential periods: heating, intermediate, cooling, intermediate and heating. During heating and cooling periods, the IAT is controlled by the heating/cooling emitters and thus their values fluctuate at 20 ± 1 °C or 26 ± 1 °C. These values can be perceived from the beginning till 1825 h, then between 3285 h and 6205 h, and at last from 7665 h to the end of this year.

Outside of the heating and cooling periods, the IAT is not HVAC controlled and thus fluctuates along with outdoor conditions (mainly OAT). The four curves in Fig. 4 shows the absorptive OFW (albedo = 0.1) results in the highest IAT values, while the reflective OFW gives the lowest ones. The largest temperature difference can be as high as 2 °C. Between the two OFW curves, the *actual* and *ideal* OVW provide more comfortable indoor environments by approaching IAT values to the range of 20–26 °C. For instance, at the beginning of spring, the IAT in a reflective OFW building can be as low as 17.8 °C. This value is under the acceptable range of human comfort and is considered as overcool discomfort. Distinguished from the two OFW, the ideal OVW can uplift this value to 18.2 °C, i.e. closer to the comfort target 20 °C. Similar comfort improvement can be perceived at the beginning of Autumn for overheat discomfort.

To better illustrate the IAT distribution, we show in Fig. 5 the IAT distribution according to OAT exclusively during the two intermediate periods. Thanks to the *ideal* OVW, stronger concentration of IAT is located in the satisfactory comfort ranges in the sub-figure b). OFW with low reflectivity renders more overheat discomfort (sub-figure a) while that with high reflectivity (albedo = 0.8, sub-figure c) gives more overcool points under the comfort range.

DDH, DH and DHr can also reflect the discomfort during intermediate seasons. According to Table 1, deploying the *ideal* OVW results in relative discomfort hours (DHhr and DHcr) of 15.7% and 8.3% of the total intermediate season, respectively representing overcool and overheat discomforts. As distinct from this performance, using absorptive OFW only slightly reduce the overcool discomfort to 7.1% while seriously extending the overheat discomfort to 23.3%. Similarly and under the same climatic condition, the reflective OFW prolongs the overcool discomfort to 12.8% and only marginally reduce the overheat discomfort to 14.6%. Considering both overheat and overcool discomfort, the discomfort hour is the shortest for the *ideal* OVW (699 h) and longest for absorptive OFW (887 h). The *actual* OVW can already enable an overall discomfort hours to 762 h, shorter than both OFW.

Moreover, from the point of view of DDH, which in addition accounts for the discomfort degree by summing up the temperature difference, OVWs clearly supports more comfortable indoor environment. The *ideal* OVW considerably reduces the overheat discomfort degree hours (DDHh) to 3600 °C·h, compared with absorptive OFW that results in a DDHh of 4582 °C·h. Similar effects are valid for DDHc (overcool) values, compared with reflective OFW. To sum up, by using the ideal

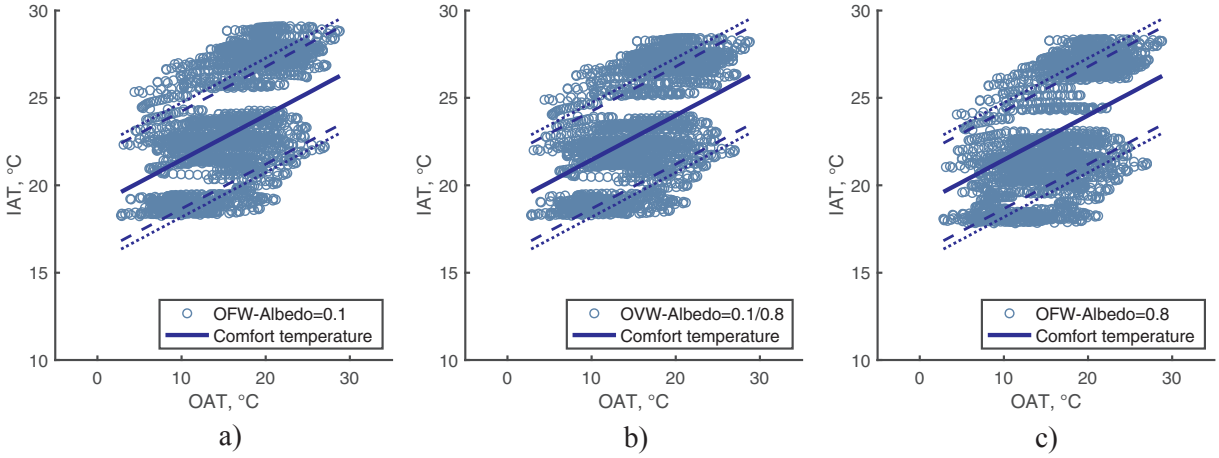

Fig. 5. Thermal comfort comparison by IAT distribution with respect to OAT, case of Shanghai Solid line (—): comfort temperature, dashed line (----): 90% satisfactory comfort range, dotted line (····): 80% satisfactory comfort range. (a) absorptive optic fixed wall with albedo = 0.1; (b) ideal optic variable wall, with albedo ranging from 0.1 to 0.8 and (c) reflective optic fixed wall with albedo = 0.8.

OVW, the DDH can be improved by a reduction of 639–735 °C·h.

Regarding extremely hot or cold discomfort values, OVWs help to reduce the discomfort degree by approaching the extreme values to the comfort zone. This is furtherly elaborated in the Discussions section.

4.2. Case of Paris

The climatic conditions in Paris (see Fig. A1 and Fig. A2 in Supplementary Data) is very different from that of Shanghai, particularly in Summer. According to normal Paris statistic metrological data (without UHI consideration or heatwave episode), little air-conditioning demand is expected in Summer [16].

The only cooling demand in Paris, as shown in Fig. 6, appears to be 18 kWh all through the year, when the building is coated with a highly absorptive albedo (0.1). Otherwise, no cooling demand is necessary.

Regarding heating demand, the two OVW and the absorptive OFW offers quasi-equivalent values: between 860 kWh and 866 kWh. As a comparison, the reflective coated building with a fixed albedo of 0.8 requires 68 kWh more energy consumption in heating, reaching an annual demand of 934 kWh. This means a heating saving of 7.3% with OVW, taking the worst case as a baseline.

Effects of OVW on IAT comfort, as shown in Fig. 7, are similar with the case of Shanghai. The reflective OFW results in higher overcool discomfort while the building remains particularly cool during hot seasons. In contrary, the absorptive coated OFW has the opposite effect. The *actual* and *ideal* OVW offer a compromised comfort with the IAT ranging in-between the above two OFW curves. It is concluded that the actual OVW has less cooling effect than the *ideal* OVW, since some overheat discomforts are higher with the *actual* one.

Statistically, as shown in Fig. 8, the discomfort in Paris' intermediate seasons is mainly the overcool issue. It is clear that the OVW (*ideal* one, shown in subfigure b) reduces overcool discomfort by increasing the IAT temperature, compared with that of the reflective one (shown in subfigure c). The difference between the OVW and absorptive OFW, however, is less significant. This implies that the OVW remains 0.1 in most time, playing exactly the same role as the OFW who has its albedo as 0.1.

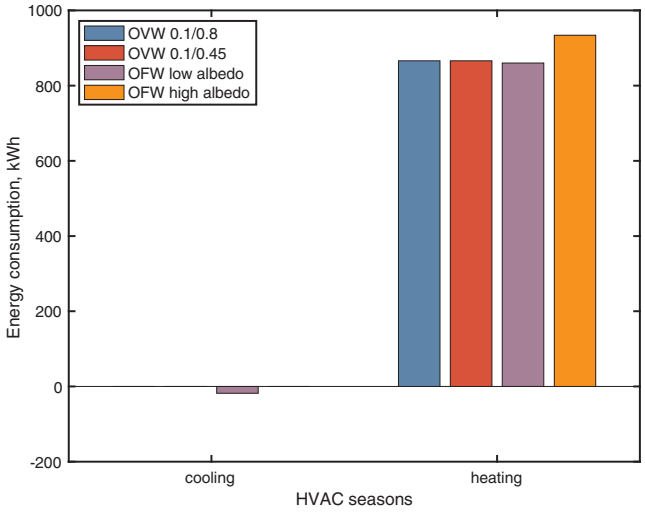

Fig. 6. Comparison of annual Heating and Cooling primary energy consumption (in kWh).

The criteria of DDH, DH and DHr, shown in Table 2, also confirm the effects of OVW in the reduction of overcool discomfort. With the absence of overheat DH, the overcool DH of the *actual* and the *ideal* OVW is respectively 1487 h and 1517 h, representing 50.9% and 52% of the total intermediate season. This is a clear improvement since a reflective OFW results in 1838 h or 62.9% of overcool discomfort during the intermediate season. This overcool aspect should be considered since many infrastructure companies are promoting the use of reflective coating as an effective measure against heatwave attacks [51,52]. Yet the side effect of the high reflective coating on heating consumption increase is non-negligible [53].

The overheat and overcool discomfort degree hours for the OVWs are also promising. We observe significant reductions of either DDHh or

Table 1
Thermal comfort comparison by DDH, DH and DHr, case of Shanghai.

Shanghai	DDHh (°C·h)	DDHc (°C·h)	DHh (h)	DHc (h)	DHhr (%)	DHcr (%)
OVW actual (0.1/0.45)	3948	2564	535	227	18.3%	7.8%
OVW ideal (0.1/0.8)	3600	2684	457	242	15.7%	8.3%
OFW Absorb (0.1)	4580	2343	679	208	23.3%	7.1%
OFW Reflect (0.8)	3402	3618	425	373	14.6%	12.8%

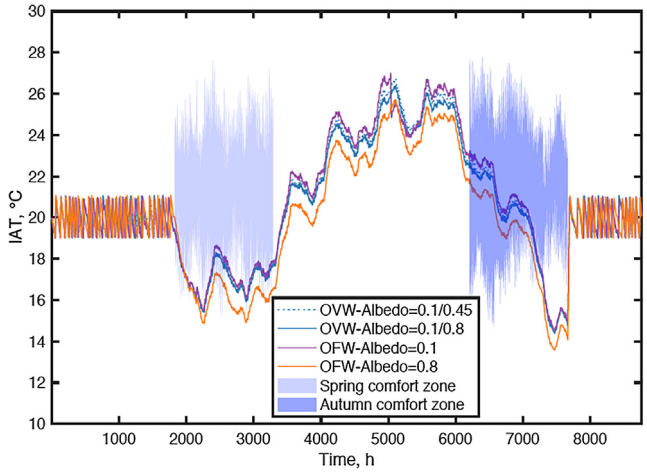

Fig. 7. Indoor air temperature all through the year, case of Paris Transition seasons during which no heating or cooling measures are shown, *actual* OVW is shown as OVW-Albedo = 0.1/0.45, and *ideal* OVW is shown as OVW-Albedo = 0.1/0.8; OFW-Albedo = 0.1 and OFW-Albedo = 0.8 are absorptive and reflective fixed albedo surface, respectively.

DDHc for the cases of OVWs. For instance, the ideal OVW enables a reduced DDHc to 9489 °C·h compared with that of a reflective OFW (11696 °C·h). Whereas the overheat DDHh benefits more from the ideal OVW with 104 °C·h other than 241 °C·h in the case of absorptive OFW.

Another comparison is made between the OVWs and the two extreme OFW cases. For instance, the absorptive OFW results in the lowest DDHc value (8817 °C·h). However, its DDHh is the highest among the four studied cases. This implies that OFW is not able to simultaneously offer benefits of less cooling in summer and less heating in winter. Whereas the ideal OVW could enable a reduction of 137 °C·h in DDHh and 2124 °C·h in DDHc, compared with the worst cases given by the two OFW.

Finally, out of our expectation, using the ideal OVW in Paris cannot reduce but increase the discomfort hours compared with using the actual OVW. As the only discomfort case (since DHh = 0), the DHcr rises from 50.9% with actual OVW to 52% with the ideal one. The possible reason behind this is the tuning temperature which is instantaneous while the delay is high in the response of IAT due to building thermal inertia. For example, in a cold-dominant intermediate season, letting more solar radiation in the day can be beneficial for the building thermal comfort later at night. However, the albedo of the tunable coating is only dependent on the outer wall surface temperature. Once this temperature exceeds the high-end tuning value, the OVW becomes instantaneously reflective. In this case, the ideal OVW offers stronger solar reflection (albedo = 0.8) than the *actual* OVW (albedo = 0.45), resulting in the reduction of desirable solar gain and correspondingly, leads to more overcool discomfort. Similar but less significant overcool effects can be observed in Table 1 for the case of Shanghai using the *ideal* OVW. Moreover, other solar regulation techniques such as electrochromic glasses [54], films [8], may also suffer from this issue.

4.3. Discussions

Comparing the application of OVW in Shanghai and Paris, our results illustrate OVW gives shorter discomfort duration (DHh and DHc) and less intensive discomfort degree hours (DDHh and DDHc) than OFWs. This confirms the functionality of *auto-regulation* thanks to its temperature responsive characteristic. Besides, the deployment of thermally responsive coating also avoids unintended effects [50] such as overheating, overcooling or water condensation by highly-emissive or highly-reflective coatings.

To provide clearer indications to architects, some points should be addressed namely to which wall the thermally responsive coating should be deployed, and under which climatic condition.

4.3.1. Wall orientation preference

Compared with the East wall, a South-orienting (or facing equator) wall receives more intensive solar radiation and is more adapted to the use of OVW. Shown in Fig. 9 and Fig. 10 are annual evolutions of south- and east-albedo for the two climatic conditions. They clearly show the more frequent optical adaptation (response) of the south side (in blue) than the east side (in red). This is partially explained by the fact that south walls receive more intense solar radiation in northern hemispheric buildings. Another reason is, compared with the south wall, the east side wall is placed under strong solar radiation in the morning when the outdoor temperature is relatively lower than the afternoon. The solar absorption in the morning is not enough to excite the tuning effect of OVW. The two reasons support the idea of using OVW by priority at the south side.

Nevertheless, it worth noting that the influence of albedo acts only during the daytime. During the night, the heat flux is only a function of the IAT and OAT, and the total wall thermal resistance. The OVW can still change its albedo property but this has no effect on the heat transfer between the building and the outdoor environment.

4.3.2. Climate adaptivity

The OVW deployment is more adapted to Shanghai climate than to

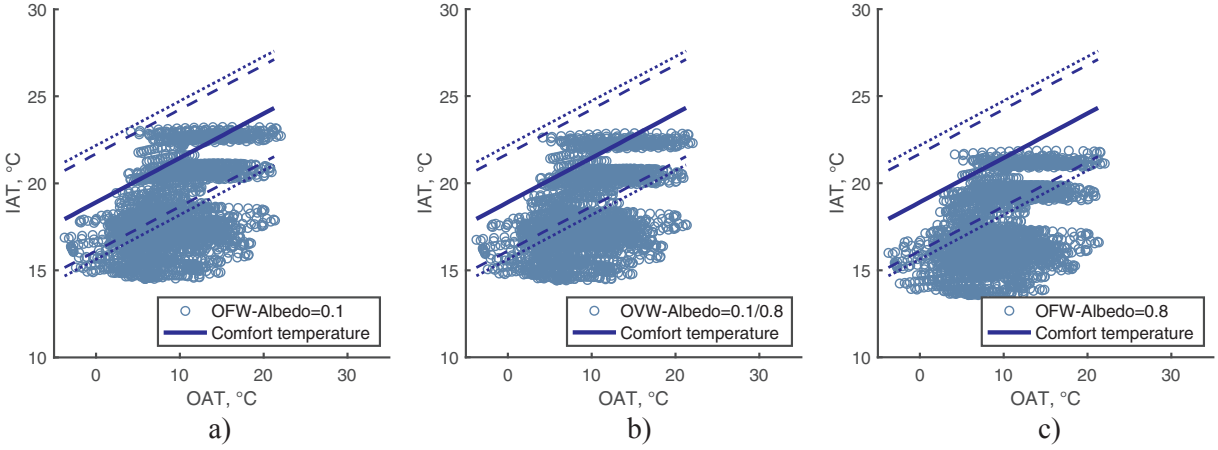

Fig. 8. Thermal comfort comparison by IAT distribution with respect to OAT, case of Paris Solid line (——): comfort temperature, dashed line (----): 90% satisfactory comfort range, dotted line (····): 80% satisfactory comfort range. (a) absorptive optic fixed wall with albedo = 0.1; (b) ideal optic variable wall, with albedo ranging from 0.1 to 0.8 and (c) reflective optic fixed wall with albedo = 0.8.

Table 2
Thermal comfort comparison by DDH, DH and DHr, case of Paris.

Paris	DDHh (°C·h)	DDHc (°C·h)	DHh (h)	DHc (h)	DHhr (%)	DHcr (%)
OVW actual (0.1/0.45)	143	9287	0	1487	0.0%	50.9%
OVW ideal (0.1/0.8)	104	9489	0	1517	0.0%	52.0%
OFW Absorb (0.1)	241	8817	0	1396	0.0%	47.8%
OFW Reflect (0.8)	22	11,696	0	1838	0.0%	62.9%

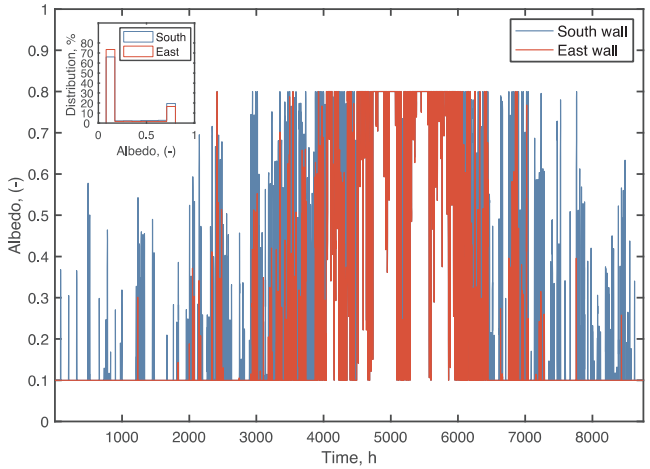

Fig. 9. Variation of albedo all through the year under Shanghai climatic conditions (ideal OVW).

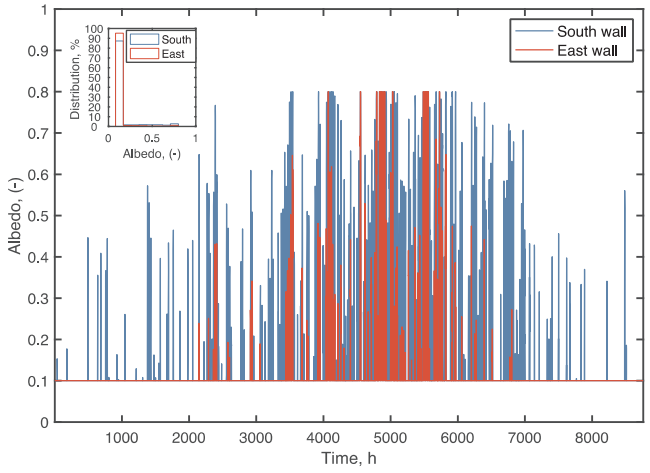

Fig. 10. Variation of albedo all through the year under Paris climatic conditions (ideal OVW).

that of Paris. As previously discussed, potential HVAC consumption saving in Shanghai is at the order of 14% while for Paris it is only 7%. In terms of albedo distribution, the histograms in Fig. 9 and Fig. 10 show different behaviors for the two cities. Globally, a high concentration in the absorptive mode (albedo = 0.1) than reflective mode is witnessed for both climates. For the case of Shanghai, South-side albedo remains at 0.1 for 67% of the year, and 0.8 for only 16% (mainly in Summer). In-between the two values, the coating is varying for a duration of 17% of a year. Meanwhile in Paris where the climate is colder, the distribution is 88% in absorptive mode, only 4% as highly reflective, and 8% in-between. In conclusion, the same OVW is doubly tuned (17% v.s. 8%) in Shanghai than in Paris, contributing to HVAC saving and better comfort.

4.3.3. Extremely overcool or overheat discomforts

The extremely high/low temperatures during intermediate seasons are closer to the acceptable comfort range thanks to OVW. Shown in Table 3 are extremely hot (IATmax) and cold (IATmin) temperatures during intermediate seasons. Compared with an absorptive wall, the IATmax in an OVW building is lower by 0.5–0.9 °C for both cities, meaning less extremely overheat. Similar effect applies to the IATmin when comparing with fixed reflective walls. This supports the effects of OVW on keeping air temperature inside stable as expected earlier in [33].

Table 3
Thermal comfort comparison by extremely hot or cold IAT during intermediate periods in Paris and Shanghai (too hot, too cold, relatively comfortable).

	Shanghai		Paris	
	IATmax (°C)	IATmin (°C)	IATmax (°C)	IATmin (°C)
OVW actual (0.1/0.45)	28.4	18.2	22.9	14.4
OVW ideal (0.1/0.8)	28.0	18.2	22.7	14.4
OFW Absorb (0.1)	29.1	18.2	23.2	14.5
OFW Reflect (0.8)	28.4	17.8	21.9	13.6

4.3.4. Limitations and future research

The first acknowledged limitation of this study is the use of the lumped model considering the whole 75 m^2 building as a single zone. By using this simplified method, the effect of OVW could be *under-estimated* since the adjusted heat flux from solar-exposed walls is then shared by all the space. While it is recognized that zoning methods have a significant impact on the building energy simulation [55], separating differently oriented rooms as well as considering occupancy's behaviour is among our priority investigations. A number of more sophisticated physics-based or data-based simulation approaches are available [56].

Secondly, building thermal mass as well as insulation are fixed in the current study while there could be a variety of buildings in the existing stock. Highly insulated building under recent building thermal codes would benefit less from the tuning effect. This can be explained through Eq. (1) in which the heat flux Φ is less significant in case of thick and efficient insulation layer. High thermal inertia in heavy buildings plays the role of thermal energy storage [57,58], which may delay the tuning effect of OVW. Consequently, a future sensitivity analysis may give guidance to a larger number of buildings regarding the OVW technology.

Last, the climatic adaptivity study could be extended to other climatic conditions. Accordingly, coating materials with most appropriate tuning temperature ranges can be developed, following the characterization methods of Wang et al., 2018 [32].

5. Conclusions

The main contribution of this study is to demonstrate the effects of OVW on the building heating and cooling energy saving as well as the thermal comfort improvement during intermediate seasons. Shanghai and Paris, two distinct but representative climatic conditions, are simulated based on a same building plan. The effects of OVW and its deployment strategies are discussed.

Integration study in Shanghai and Paris shows better adaptability of this technology in the climatic condition of Shanghai, where heating and cooling demands are comparable. Heating and cooling demands are

respectively reduced by 14.8% and 14.2% with the future *ideal* OVW. Comparatively, Paris has a cold dominant weather and the ideal OVW has equivalent effect as that of highly absorptive wall in terms of heating consumption. Also, the cold demand remains zero in the cases of OVW and reflective OFW, while it becomes non-zero once the OFW of an albedo of 0.1 is used. Whatsoever, for both cities, the thermal discomfort degree-hours during intermediate seasons are both reduced thanks to the deployment of OVW.

Comparing the two cases of OVW, the *actual* coating (albedo = 0.1/0.45) allows less overall energy saving than the *ideal* one (albedo = 0.1/0.8), particularly in terms of cooling load under the Shanghai climate. On the contrary, an unexpected result is witnessed: the increase of discomfort hours with the adoption of the *ideal* OVW, comparing with the *actual* OVW, under the climatic condition of Paris. This is primarily due to the albedo adjustment with temperature is quasi-instantaneous while the response of building thermal mass is slow. A future tuning coating should depend not only on temperature but a multiple of parameters related to buildings.

Acknowledgements

This study received financial support from the French Ministry of Europe and Foreign Affairs (MEAE), through the PHC Xu Guangqi program (No: 41269UL, 2018) and the Jeunes Talents France-Chine program (No: 925116B, 2018). This study also received financial supports from the Natural Science Foundation of China within the project No 51306023. The authors would like to acknowledge the support from Advanced Catalysis and Green Manufacturing Collaborative Innovation Center of Jiangsu, China.

Appendix A. Supplementary material

Supplementary data to this article can be found online at https://doi.org/10.1016/j.apenergy.2019.113506.

References

[1] Bourdeau M, Guo X, Nefzaoui E. Buildings energy consumption generation gap: A post-occupancy assessment in a case study of three higher education buildings. Energy Build 2018;159:600–11. https://doi.org/10.1016/j.enbuild.2017.11.062.
[2] Yang L, Yan H, Lam JC. Thermal comfort and building energy consumption implications - A review. Appl Energy 2014. https://doi.org/10.1016/j.apenergy.2013.10.062.
[3] Weng Q. Thermal infrared remote sensing for urban climate and environmental studies: Methods, applications, and trends. ISPRS J Photogramm Remote Sens 2009. https://doi.org/10.1016/j.isprsjprs.2009.03.007.
[4] Rossi F, Castellani B, Presciutti A, Morini E, Filipponi M, Nicolini A, et al. Retroreflective façades for urban heat island mitigation: Experimental investigation and energy evaluations. Appl Energy 2015. https://doi.org/10.1016/j.apenergy.2015.01.129.
[5] Aktacir MA, Büyükalaca O, Yilmaz T. A case study for influence of building thermal insulation on cooling load and air-conditioning system in the hot and humid regions. Appl Energy 2010. https://doi.org/10.1016/j.apenergy.2009.05.008.
[6] Al-Sanea SA, Zedan MF. Improving thermal performance of building walls by optimizing insulation layer distribution and thickness for same thermal mass. Appl Energy 2011. https://doi.org/10.1016/j.apenergy.2011.02.036.
[7] Daouas N. A study on optimum insulation thickness in walls and energy savings in Tunisian buildings based on analytical calculation of cooling and heating transmission loads. Appl Energy 2011. https://doi.org/10.1016/j.apenergy.2010.07.030.
[8] Li C, Tan J, Chow TT, Qiu Z. Experimental and theoretical study on the effect of window films on building energy consumption. Energy Build 2015. https://doi.org/10.1016/j.enbuild.2015.04.025.
[9] Wang M, Peng J, Li N, Yang H, Wang C, Li X, et al. Comparison of energy performance between PV double skin facades and PV insulating glass units. Appl Energy 2017. https://doi.org/10.1016/j.apenergy.2017.03.019.
[10] Hong T, Koo C, Kim J, Lee M, Jeong K. A review on sustainable construction management strategies for monitoring, diagnosing, and retrofitting the building's dynamic energy performance: Focused on the operation and maintenance phase. Appl Energy 2015. https://doi.org/10.1016/j.apenergy.2015.06.043.
[11] Cui B, Gao DC, Wang S, Xue X. Effectiveness and life-cycle cost-benefit analysis of active cold storages for building demand management for smart grid applications. Appl Energy 2015. https://doi.org/10.1016/j.apenergy.2015.03.041.
[12] Self SJ, Reddy BV, Rosen MA. Geothermal heat pump systems: Status review and comparison with other heating options. Appl Energy 2013. https://doi.org/10.1016/j.apenergy.2012.01.048.
[13] Guo X, Goumba AP. Air source heat pump for domestic hot water supply: Performance comparison between individual and building scale installations. Energy 2018;164:794–802. https://doi.org/10.1016/j.energy.2018.09.065.
[14] Wang Y, Zhao FY, Kuckelkorn J, Spliethoff H, Rank E. School building energy performance and classroom air environment implemented with the heat recovery heat pump and displacement ventilation system. Appl Energy 2014. https://doi.org/10.1016/j.apenergy.2013.09.020.
[15] Thalfeldt M, Kurnitski J, Latõšov E. Exhaust air heat pump connection schemes and balanced heat recovery ventilation effect on district heat energy use and return temperature. Appl Therm Eng 2018. https://doi.org/10.1016/j.applthermaleng.2017.09.033.
[16] Guo X, Hendel M. Urban water networks as an alternative source for district heating and emergency heat-wave cooling. Energy 2018;145:79–87. https://doi.org/10.1016/j.energy.2017.12.108.
[17] Trillat-Berdal V, Souyri B, Achard G. Coupling of geothermal heat pumps with thermal solar collectors. Appl Therm Eng 2007. https://doi.org/10.1016/j.applthermaleng.2006.07.022.
[18] Buonomano A, Calise F, Palombo A, Vicidomini M. Energy and economic analysis of geothermal-solar trigeneration systems: A case study for a hotel building in Ischia. Appl Energy 2015. https://doi.org/10.1016/j.apenergy.2014.10.076.
[19] Sepehri A, Sarrafzadeh M-H. Effect of nitrifiers community on fouling mitigation and nitrification efficiency in a membrane bioreactor. Chem Eng Process - Process Intensif 2018;128:10–8. https://doi.org/10.1016/J.CEP.2018.04.006.
[20] Engström RE, Howells M, Destouni G, Bhatt V, Bazilian M, Rogner H-H. Connecting the resource nexus to basic urban service provision – with a focus on water-energy interactions in New York City. Sustain Cities Soc 2017;31:83–94. https://doi.org/10.1016/j.scs.2017.02.007.
[21] Goumba A, Chiche S, Guo X, Colombert M, Bonneau P. Recov'Heat: An estimation tool of urban waste heat recovery potential in sustainable cities. AIP Conf. Proc. 2017;1814. https://doi.org/10.1063/1.4976257.
[22] Liu S, Kwok YT, Lau KK-L, Chan PW, Ng E. Investigating the energy saving potential of applying shading panels on opaque façades: A case study for residential buildings in Hong Kong. Energy Build 2019;193:78–91. https://doi.org/10.1016/J.ENBUILD.2019.03.044.
[23] Ghosh A, Norton B. Advances in switchable and highly insulating autonomous (self-powered) glazing systems for adaptive low energy buildings. Renew Energy 2018;126:1003–31. https://doi.org/10.1016/J.RENENE.2018.04.038.
[24] Sun Y, Wu Y, Wilson R. A review of thermal and optical characterisation of complex window systems and their building performance prediction. Appl Energy 2018;222:729–47. https://doi.org/10.1016/J.APENERGY.2018.03.144.
[25] Zhang Y, Long E, Li Y, Li P. Solar radiation reflective coating material on building envelopes: Heat transfer analysis and cooling energy saving. Energy Explor Exploit 2017;35:748–66. https://doi.org/10.1177/0144598717716285.
[26] Pisello AL, Castaldo VL, Piselli C, Pignatta G, Cotana F. Combined Thermal Effect of Cool Roof and Cool Façade on a Prototype Building. Energy Procedia 2015;78:1556–61. https://doi.org/10.1016/J.EGYPRO.2015.11.205.
[27] Morini E, Castellani B, Presciutti A, Filipponi M, Nicolini A, Rossi F. Optic-energy performance improvement of exterior paints for buildings. Energy Build 2017;139:690–701. https://doi.org/10.1016/j.enbuild.2017.01.060.
[28] Goldstein EA, Raman AP, Fan S. Sub-ambient non-evaporative fluid cooling with the sky. Nat Energy 2017. https://doi.org/10.1038/nenergy.2017.143.
[29] Jelle BP, Kalnæs SE, Gao T. Low-emissivity materials for building applications: A state-of-the-art review and future research perspectives. Energy Build 2015;96:329–56. https://doi.org/10.1016/J.ENBUILD.2015.03.024.
[30] Taha M, Walia S, Ahmed T, Headland D, Withayachumnankul W, Sriram S, et al. Insulator–metal transition in substrate-independent VO2 thin film for phase-change devices. Sci Rep 2017;7:17899. https://doi.org/10.1038/s41598-017-17937-3.
[31] Clever coating opens door to smart windows | Printed Electronics World n.d. https://www.printedelectronicsworld.com/articles/13823/clever-coating-opens-door-to-smart-windows [accessed September 21, 2018].
[32] Wang C, Zhu Y, Qu J, Hu HD. Automatic air temperature control in a container with an optic-variable wall. Appl Energy 2018;224:671–81. https://doi.org/10.1016/j.apenergy.2018.05.018.
[33] Wang C, Guo X, Zhu Y. Energy saving with Optic-Variable Wall for stable air temperature control. Energy 2019;173:38–47. https://doi.org/10.1016/j.energy.2019.02.051.
[34] Asadi E, da Silva MG, Antunes CH, Dias L, Glicksman L. Multi-objective optimization for building retrofit: A model using genetic algorithm and artificial neural network and an application. Energy Build 2014;81:444–56. https://doi.org/10.1016/J.ENBUILD.2014.06.009.
[35] Ramakrishnan S, Wang X, Sanjayan J, Wilson J. Thermal performance of buildings integrated with phase change materials to reduce heat stress risks during extreme heatwave events. Appl Energy 2017;194:410–21. https://doi.org/10.1016/J.APENERGY.2016.04.084.
[36] Dabaieh M, Wanas O, Hegazy MA, Johansson E. Reducing cooling demands in a hot dry climate: A simulation study for non-insulated passive cool roof thermal performance in residential buildings. Energy Build 2015;89:142–52. https://doi.org/10.1016/J.ENBUILD.2014.12.034.
[37] Zhang Y, Lin K, Zhang Q, Di H. Ideal thermophysical properties for free-cooling (or heating) buildings with constant thermal physical property material. Energy Build 2006;38:1164–70. https://doi.org/10.1016/J.ENBUILD.2006.01.008.
[38] Lin Y, Zhou S, Yang W, Shi L, Li C-Q. Development of building thermal load and discomfort degree hour prediction models using data mining approaches. Energies 2018;11:1570. https://doi.org/10.3390/en11061570.

[39] Fanger PO. Thermal comfort. Analysis and applications in environmental engineering. Therm Comf Anal Appl Environ Eng 1970.
[40] Comité Européen de Normalisation. Indoor Environmental Input Parameters for Design and Assessment of Energy Performance of Buildings Addressing Indoor Air Quality, Thermal Environment, Lighting and Acoustics. 2007. http://doi.org/10.1520/E2019-03R13.Copyright.
[41] Allab Y, Pellegrino M, Guo X, Nefzaoui E, Kindinis A. Energy and comfort assessment in educational building: Case study in a French university campus. Energy Build 2017;143:202–19. https://doi.org/10.1016/j.enbuild.2016.11.028.
[42] International Organization for Standardization. Ergonomics of the thermal environment- Analytical determination and interpretation of thermal comfort using PMV and PPD indices and local thermal comfort criteria. 2005. http://doi.org/10.1016/j.ecoenv.2016.12.003.
[43] Olesen BW, Parsons KC. Introduction to thermal comfort standards and to the proposed new version of EN ISO 7730. Energy Build 2002;34:537–48. https://doi.org/10.1016/S0378-7788(02)00004-X.
[44] Jörn von Grabe I. A preliminary cognitive model for the prediction of energy-relevant human interaction with buildings. Cogn Syst Res 2017. https://doi.org/10.1016/j.cogsys.2017.11.005.
[45] de Dear RJ, Brager GS. Developing an adaptive model of thermal comfort and preference. ASHRAE Trans 1998;104.
[46] de Dear R, Brager GS. The adaptive model of thermal comfort and energy conservation in the built environment. Int J Biometeorol 2001;45:100–8.
[47] Klein SA. TRNSYS 17: A Transient System Simulation Program. Sol Energy Lab Univ Wisconsin, Madison, USA 2010;1:1–5.
[48] CSTB. Meteonorm, TRNSYS package, http://logiciels.cstb.fr/Thermique-METEONORM 2012.
[49] Pan J, Zou R, Jin F. Experimental study on specific heat of concrete at high temperatures and its influence on thermal energy storage. Energies 2017;10:33. https://doi.org/10.3390/en10010033.
[50] Simpson A, Fitton R, Rattigan IG, Marshall A, Parr G, Swan W. Thermal performance of thermal paint and surface coatings in buildings in heating dominated climates. Energy Build 2019. https://doi.org/10.1016/J.ENBUILD.2019.04.027.
[51] Nazarian N, Dumas N, Kleissl J, Norford L. Effectiveness of cool walls on cooling load and urban temperature in a tropical climate. Energy Build 2019;187:144–62. https://doi.org/10.1016/J.ENBUILD.2019.01.022.
[52] Qiu T, Wang G, Xu Q, Ni G. Study on the thermal performance and design method of solar reflective–thermal insulation hybrid system for wall and roof in Shanghai. Sol Energy 2018;171:851–62. https://doi.org/10.1016/J.SOLENER.2018.07.036.
[53] Collins M, Dempsey S. Residential energy efficiency retrofits: potential unintended consequences. J Environ Plan Manag 2018:1–16. https://doi.org/10.1080/09640568.2018.1509788.
[54] Cannavale A, Martellotta F, Cossari P, Gigli G, Ayr U. Energy savings due to building integration of innovative solid-state electrochromic devices. Appl Energy 2018;225:975–85. https://doi.org/10.1016/J.APENERGY.2018.05.034.
[55] Chen Y, Hong T. Impacts of building geometry modeling methods on the simulation results of urban building energy models. Appl Energy 2018;215:717–35. https://doi.org/10.1016/J.APENERGY.2018.02.073.
[56] Bourdeau M, Zhai X-Q, Nefzaoui E, Guo X, Chatellier P. Modelling and forecasting building energy consumption: a review of data-driven techniques. Sustain Cities Soc 2019;48:101533https://doi.org/10.1016/j.scs.2019.101533.
[57] Leccese F, Salvadori G, Asdrubali F, Gori P. Passive thermal behaviour of buildings: Performance of external multi-layered walls and influence of internal walls. Appl Energy 2018;225:1078–89. https://doi.org/10.1016/J.APENERGY.2018.05.090.
[58] Finck C, Li R, Kramer R, Zeiler W. Quantifying demand flexibility of power-to-heat and thermal energy storage in the control of building heating systems. Appl Energy 2018;209:409–25. https://doi.org/10.1016/J.APENERGY.2017.11.036.